THE SECULAR EVOLUTION OF A CLOSE RING-SATELLITE SYSTEM: THE EXCITATION OF SPIRAL DENSITY WAVES AT A NEARBY GAP EDGE

Joseph M. Hahn
Space Science Institute, 10500 Loring Drive, Austin, TX 78750; jhahn@spacescience.org

ABSTRACT

The Lagrange planetary equations are used to study secular evolution of a small, eccentric satellite that orbits within a narrow gap in a broad, self-gravitating planetary ring. These equations show that the satellite's secular perturbations of the ring will excite a very long wavelength spiral density wave that propagates away from the gap's outer edge. The amplitude of these waves, as well as their dispersion relation, are derived here. That dispersion relation reveals that a planetary ring can sustain two types of density waves: long waves that, in Saturn's A ring, would have wavelengths of $\lambda \sim O(100)$ km and short waves that tend to be very nonlinear and are expected to quickly damp. The excitation of these waves also transports angular momentum from the ring to the satellite in a way that damps the satellite's eccentricity e, which also tends to reduce the amplitude of subsequent waves. The rate of eccentricity damping due to this wave action is then compared to the rates at which the satellite's Lindblad and corotation resonances alter the satellite's e. These results are then applied to the gap-embedded Saturnian satellites Pan and Daphnis, and the long-term stability of their eccentricities is assessed.

Subject heading: planets: rings

1. INTRODUCTION

The following considers the secular gravitational perturbations that are exerted between a small eccentric satellite and a nearby planetary ring. This investigation is also a followup to the study described in Hahn (2007) which examined the secular evolution of a small inclined satellite. There it was shown that the inclined satellite would launch a very long wavelength spiral bending wave at the ring's nearby edge. Since the excitation of the bending wave also communicates in-plane angular momentum from the satellite to the ring, that ring-satellite interaction resulted in a very vigorous damping of the satellite's inclination. A related problem was also considered by Goldreich & Sari (2003), who showed that an eccentric perturber orbiting in a gap in a pressure-supported gas disk will launch density waves at the gap's edge having such a long wavelength that a global standing wave emerges in the disk. The work described below considers a related but distinct problem, that of an eccentric satellite orbiting in a narrow gap in a self-gravitating planetary ring. Here we show that the secular perturbations from the eccentric satellite also launches relatively long wavelength density waves at the gap's outer edge. The principal goal of this study will be to derive the amplitude of these waves and their dispersion relation, which in turn will yield other useful properties, such as the wavenumber and the waves' group velocity. Since the mathematics of this density wave problem is very similar to that already developed for bending waves, the derivations presented here will be succinct. However, the reader interested in a more verbose description of a similar problem is referred to Hahn (2007).

Another goal of this effort will be to derive the rate at which the satellite's eccentricity e is altered by the excitation of these density waves at the gap's edge. This is of interest because the satellite's e also varies due to its many Lindblad resonances in the ring, which tend to pump up the satellite's e, while its many corotation resonances in the ring tend to damp the satellite's e (Goldreich & Tremaine 1981, 1982). Although e-damping due to the corotation torque can dominate over e-excitation from the Lindblad torque, the long-term stability of the satellite's eccen-

tricity is still uncertain since the corotation torque is operative only when these particular resonances are not saturated. Our purpose here is to determine whether the secular interaction described below is also a stabilizing process that leads to a net damping of the satellite's eccentricity.

The following section begins with the Lagrange planetary equations, which are used to derive the amplitude of these waves and their dispersion relation. Section 3 then uses those results to determine the rate at which the satellite's eccentricity evolves in response to the wave it launches at the gap edge. Those analytic results are then confirmed in § 4 via a numerical simulation of these waves, with conclusions reported in § 5.

2. EQUATIONS OF MOTION

Consider a planetary ring that is perturbed by a single satellite, with both orbiting an oblate planet. The Lagrange planetary equations give the rates at which a ring particle's orbital eccentricity e and longitude of periapse $\tilde{\omega}$ vary with time t due to these perturbations (Brouwer & Clemence 1961; Murray & Dermott 1999),

$$\dot{e} \simeq -\frac{1}{na^2 e}\frac{\partial R}{\partial \tilde{\omega}}, \quad \dot{\tilde{\omega}} \simeq \frac{1}{na^2 e}\frac{\partial R}{\partial e}, \quad (1)$$

where R is the disturbing function for a small ring particle having a semimajor axis a and mean motion $n \simeq (GM/a^3)^{1/2}$, where G is the gravitation constant and M is the mass of the central planet, and all eccentricities are small, $e \ll 1$. The total disturbing function for a ring particle is $R = R_{\mathrm{disk}} + R_{\mathrm{sat}} + R_{\mathrm{obl}}$, where the three terms account for the gravitational perturbations that are due to the ring's gravity (which is treated here as a broad disk), the satellite's perturbations, and that due to the planet's oblate figure. The particle's equation of motion is thus the sum of three parts,

$$\dot{e} = \dot{e}\big|_{\mathrm{disk}} + \dot{e}\big|_{\mathrm{sat}}, \quad \dot{\tilde{\omega}} = \dot{\tilde{\omega}}\big|_{\mathrm{disk}} + \dot{\tilde{\omega}}\big|_{\mathrm{sat}} + \dot{\tilde{\omega}}\big|_{\mathrm{obl}}, \quad (2)$$
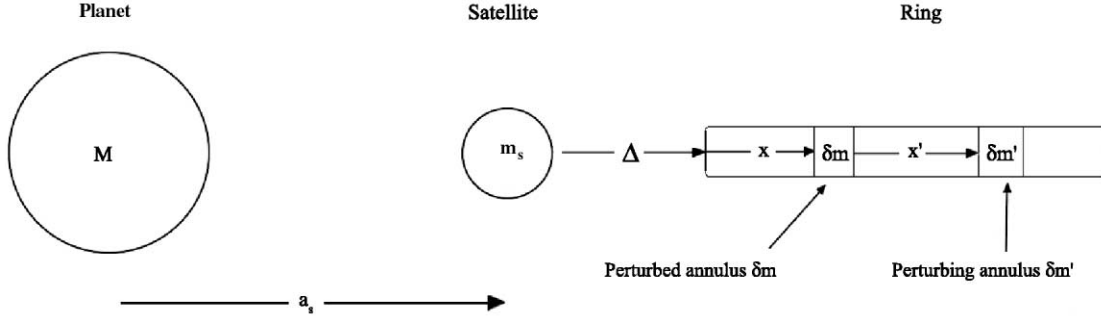
1569

FIG. 1.—Schematic showing the geometry of the ring-satellite system seen edge-on. A satellite of mass m_s and semimajor axis a_s orbits interior to a broad planetary ring that extends to infinity. The satellite's distance from the ring's inner edge is Δ in units of the satellite's semimajor axis a_s. A perturbed annulus in the ring has mass δm, and it lies a fractional distance x away from the ring's inner edge, while the perturbing ring has mass $\delta m'$ and lies a fractional distance x' from the perturbed ring.

noting that oblateness does not alter eccentricities. And because we are only dealing with the system's secular perturbations, the system's semimajor axes a are all constant (Brouwer & Clemence 1961).

The amplitude of a spiral density wave that is in a steady state does not vary with time, so the disk eccentricities obey $\dot{e}(a) = 0$ throughout the disk. A persistent spiral pattern must also rotate with a constant angular velocity ω, so

$$\dot{e}\big|_{\text{disk}} = -\dot{e}\big|_{\text{sat}}, \tag{3a}$$

$$\omega = \dot{\tilde{\omega}}\big|_{\text{disk}} + \dot{\tilde{\omega}}\big|_{\text{sat}} + \dot{\tilde{\omega}}\big|_{\text{obl}} = \text{const.} \tag{3b}$$

These equations are used to obtain the wave amplitude $e(a)$ throughout the disk and the waves' dispersion relation $\omega(k)$ as a function of the wavenumber k.

2.1. Wave Amplitude

First, calculate the rate at which the planetary ring perturbs itself. This ring is treated as a broad disk composed of many narrow, concentric annuli that have a mass $\delta m(a)$, eccentricity $e(a)$, and longitude of periapse $\tilde{\omega}(a)$ that are regarded as functions of the rings' semimajor axes a. Each annulus also has a half-thickness h that is due to the ring particles' dispersion velocity. Now suppose that the annulus at a is perturbed by another annulus of mass $\delta m'$ and radius a'; the perturbed annulus will then have a disturbing function

$$\delta R = \frac{G\delta m'}{4a}\left[\frac{1}{2}f(\alpha)e^2 + g(\alpha)ee'\cos(\tilde{\omega} - \tilde{\omega}')\right], \tag{4}$$

where a, e, and $\tilde{\omega}$ are the orbit elements of the perturbed annulus, the primed quantities refer to the perturbing annulus, and the $f(\alpha)$ and $g(\alpha)$ functions are

$$f(\alpha) = \alpha\tilde{b}_{3/2}^{(1)}(\alpha) - 6\mathfrak{h}^2\alpha^2\tilde{b}_{5/2}^{(0)}(\alpha), \tag{5a}$$

$$g(\alpha) = -\alpha\tilde{b}_{3/2}^{(2)}(\alpha) + 6\mathfrak{h}^2\alpha^2\tilde{b}_{5/2}^{(1)}(\alpha), \tag{5b}$$

which depend on the semimajor axis ratio $\alpha = a'/a$ and the disk's dimensionless scale height $\mathfrak{h} = h/a \ll 1$, which is presumed small. This disturbing function is derived in Hahn (2003) and it differs somewhat from the more familiar disturbing function for a point-mass perturber due to the annuli's finite thickness h, which also softens the Laplace coefficients that appear in δR. Those softened Laplace coefficients are

$$\tilde{b}_s^{(m)}(\alpha) = \frac{2}{\pi}\int_0^\pi \frac{\cos(m\varphi)d\varphi}{[(1 + \alpha^2)(1 + \mathfrak{h}^2) - 2\alpha\cos\varphi]^s}. \tag{6}$$

Note that when the annuli are infinitesimally thin, $\mathfrak{h} \to 0$, and the softened Laplace coefficients $\tilde{b}_s^{(m)}(\alpha)$ are equivalent to the conventional Laplace coefficients $b_s^{(m)}(\alpha)$, for which $f(\alpha) \to \alpha b_{3/2}^{(1)}(\alpha)$ and $g(\alpha) \to -\alpha b_{3/2}^{(2)}(\alpha)$, and the disturbing function δR becomes equivalent to that due to a point perturber of mass $\delta m'$ (e.g., Brouwer & Clemence 1961).

The perturbing ring's mass is $\delta m' = 2\pi\sigma'a'\,da'$, where $\sigma' = \sigma(a')$ is the mass surface density of the perturbing annulus of radius a' and radial width da'. The perturbing ring's semimajor axis is written $a' = a(1 + x')$, where $x' = (a' - a)/a = \alpha - 1$ is the fractional distance between the perturbing ring a' and the perturbed ring a. Also define the normalized disk mass as $\mu_d(a) \equiv \pi\sigma a^2/M$, so that the factor $G\delta m'/4a$ in equation (4) becomes $\mu_d'(na)^2dx'/2\alpha$, where $dx' = da'/a$ is the perturbing ring's fractional width. The disturbing function for ring a due to perturbations from ring a', equation (4), then becomes

$$\delta R = \frac{1}{2}\mu_d'(na)^2\alpha^{-1}\left[\frac{1}{2}f(x')e^2 + g(x')ee'\cos(\tilde{\omega} - \tilde{\omega}')\right]dx', \tag{7}$$

where $f(x')$ and $g(x')$ are shorthand for equations (5) evaluated at $\alpha = 1 + x'$. Inserting this into equation (1) then shows that ring a' alters the eccentricity of ring a at the rate

$$\delta\dot{e} = -\frac{1}{na^2e}\frac{\partial(\delta R)}{\partial\tilde{\omega}} = \frac{1}{2}\mu_d'n\alpha^{-1}g(x')e'\sin(\tilde{\omega} - \tilde{\omega}')dx'. \tag{8}$$

2.1.1. Ring-Disk Evolution

The total rate at which the entire disk alters the eccentricity of ring a is the above with x' integrated across the disk, so $\dot{e}\big|_{\text{disk}} = \int_{\text{disk}}\delta\dot{e}$. For the moment, consider a one-sided disk, one that orbits wholly exterior to the satellite, where Δ is the fractional distance between the satellite's orbit and the disk's inner edge. The geometry is sketched in Figure 1, which shows that the integration variable x' then ranges from $-x$ to $+\infty$, so the ring's eccentricity varies at the rate

$$\dot{e}\big|_{\text{disk}} = \int_{\text{disk}}\delta\dot{e} = \frac{1}{2}n\int_{-x}^\infty \mu_d'(x')\alpha^{-1}g(x')e'\sin(\tilde{\omega} - \tilde{\omega}')dx'. \tag{9}$$

This integral will be dominated by the contributions from nearby annuli that lie a small distance x' away. In the $|x'| \ll 1$, $\mathfrak{h} \ll 1$

limit, the softened Laplace coefficients that appear in the $g(\alpha)$ function, equation (5b), are (Hahn 2003)

$$\tilde{b}_{3/2}^{(m)}(x') \simeq \frac{2}{\pi(x'^2 + 2\mathfrak{h}^2)}, \qquad (10a)$$

$$\tilde{b}_{5/2}^{(m)}(x') \simeq \frac{4}{3\pi(x'^2 + 2\mathfrak{h}^2)^2}, \qquad (10b)$$

so $\alpha^{-1} g(\alpha)$ in equation (9) becomes

$$\alpha^{-1} g(\alpha) \simeq -\frac{2}{\pi} \frac{x'^2 - 2\mathfrak{h}^2}{(x'^2 + 2\mathfrak{h}^2)^2} \qquad (11)$$

in this approximation. Because of the steep dependence of $g(\alpha)$ on x', we can replace the eccentricity $e'(x')$ and disk mass $\mu_d'(x')$ in equation (9) with their values evaluated at the perturbed ring, which lies at $x' = 0$, so $e' \simeq e$ and $\mu_d' \simeq \mu_d = \pi\sigma a^2/M$, which are then pulled out of the integral so that

$$\dot{e}|_{\mathrm{disk}} \simeq -\frac{1}{\pi} \mu_d en \int_{-x}^{\infty} \frac{x'^2 - 2\mathfrak{h}^2}{(x'^2 + 2\mathfrak{h}^2)^2} \sin(\tilde{\omega} - \tilde{\omega}') dx'. \qquad (12)$$

A spiral wave will have a wavelength $\lambda \simeq 2\pi/|k|$, where $k = -\partial\tilde{\omega}/\partial a$ is the wavenumber of the spiral density wave. Thus, the $\tilde{\omega} - \tilde{\omega}'$ in equation (12) can also be written as

$$\tilde{\omega} - \tilde{\omega}'(a') = -\int_{a'}^{a} k(r) dr. \qquad (13)$$

However, most of the contribution to the integral in equation (12) will be due to nearby annuli that lie a wavelength λ away. But if k also varies slowly with a, then it can be treated as a constant over that wavelength, so equation (13) is $\tilde{\omega} - \tilde{\omega}' \simeq -k(a - a') = kax'$, and equation (12) then becomes

$$\dot{e}|_{\mathrm{disk}} \simeq -\frac{1}{\pi} ka\mu_d en \int_{-|k|ax}^{\infty} \frac{y^2 - H^2}{(y^2 + 2H^2)^2} \sin(y) dy$$

$$\equiv -\frac{1}{\pi} A_H'(|k|ax) ka\mu_d en \qquad (14)$$

after replacing the x' integration variable with $y = |k|ax'$, which is the distance from the ring edge in units of 2π wavelengths, and replacing the disk's scale height $\mathfrak{h}$ with $H \equiv \sqrt{2}\mathfrak{h}|k|a$, which is roughly the disk's vertical thickness in wavelength units. In the above, the function $A'(z)$ is

$$A_H'(z) = \int_{z}^{\infty} \frac{y^2 - H^2}{(y^2 + H^2)^2} \sin y \, dy, \qquad (15)$$

noting that equation (14) is also odd in y. We will be interested in a disk whose vertical thickness is small compared to the wavelength, so $H \ll 1$, and $A_H'(z) \simeq \sin(z)/z - \mathrm{Ci}(z)$, where $\mathrm{Ci}(z)$ is the cosine integral of Abramowitz & Stegun (1972). Far downstream, where $z \gg 1$, $\mathrm{Ci}(z) \simeq \sin(z)/z - \cos(z)/z^2 + O(z^{-3})$ (Abramowitz & Stegun 1972), so

$$A_H'(z) \simeq \frac{\cos(z)}{z^2} \qquad (16)$$

downstream. Evidently, $A_H'(z)$ is very similar to the $A_H(z)$ function of Hahn (2007) which is also plotted in Figure 2 there.

Also keep in mind that equation (14) was derived with the understanding that the wavenumber k varies little over a single

wavelength. Section 2.2.3 will quantify when that assumption breaks down.

2.1.2. Ring-Satellite Evolution and the Wave Amplitude

The ring at semimajor axis a is also perturbed by the satellite, and the disturbing function R_s due to the satellite is equation (4) with $\delta m'$ replaced by the satellite's mass m_s, which can be written

$$R_s = \frac{1}{4} \mu_s (na)^2 \left[\frac{1}{2} f(\alpha) e^2 + g(\alpha) e e_s \cos(\tilde{\omega} - \tilde{\omega}_s) \right], \qquad (17)$$

where $\mu_s = m_s/M$ is the satellite's mass in units of the central planet's mass and $\alpha = a_s/a = (1 + \Delta + x)^{-1} \simeq 1 - (\Delta + x)$. The satellite's perturbation causes the ring's eccentricity to vary at the rate

$$\dot{e}|_{\mathrm{sat}} = -\frac{1}{na^2 e} \frac{\partial R_s}{\partial\tilde{\omega}} = \frac{1}{4} \mu_s ng(\alpha) e_s \sin(\tilde{\omega} - \tilde{\omega}_s). \qquad (18)$$

The perturbed ring lies a fractional distance $x + \Delta$ away from the satellite (see Fig. 1), with both well separated so that $\Delta \gg \mathfrak{h}$. Since the ring also lies in the wave-excitation zone near the satellite,

$$g(\alpha) \simeq -\alpha \tilde{b}_{3/2}^{(2)}(\alpha) \simeq -\frac{2}{\pi(x + \Delta)^2} \qquad (19)$$

by equations (5b) and (10a). Also write the longitude difference in equation (18) as $\tilde{\omega} - \tilde{\omega}_s \simeq -kax + \phi_o$, where the angle ϕ_o allows for the possibility that the annulus nearest the satellite at $x = 0$ has a longitude of periapse that differs from the satellite's longitude $\tilde{\omega}_s$ by angle ϕ_o. Thus,

$$\dot{e}|_{\mathrm{sat}} \simeq \frac{\mu_s e_s n}{2\pi(x + \Delta)^2} \sin(kax - \phi_o) \qquad (20)$$

is the rate at which the satellite alters the ring's eccentricity.

When the wave is in steady state, the two e-excitation rates, equations (14) and (20), are balanced, which provides the amplitude of the density wave,

$$\frac{e(z)}{e_s} = \frac{|k|a}{2} \frac{\mu_s}{\mu_d} \frac{\sin(z - s_k\phi_o)}{(z + |k|a\Delta)^2 A_H'(z)}, \qquad (21)$$

where $s_k = \mathrm{sgn}(k)$ and $z = |k|ax$ is the downstream distance in units of 2π wavelengths. Now recall that $A_H'(z) \simeq \cos(z)/z^2$ far downstream where $z \gg 1$ (eq. [16]). Since the downstream wave amplitude $e(z)$ should be a finite constant for all $z \gg 1$, this then tells us that the longitude offset is $\phi_o = \pm\pi/2$, so $e/e_s \simeq -(|k|a/2)(\mu_s/\mu_d)s_k \sin\phi_o$. These eccentricities must also be positive, so $\sin\phi_o = \pm 1 = -s_k$, and the density wave amplitude then becomes

$$\frac{e}{e_s} \simeq \frac{|k_0|a\mu_s}{2\mu_d}, \qquad (22)$$

where $|k_0|$ is the initial wavenumber at $x = 0$, where the wave is excited at the disk's inner edge. An identical expression was also obtained in Hahn (2007) for the amplitude of the bending wave that an inclined satellite would launch at the ring's edge.

2.2. Dispersion Relation

Further use of the wave amplitude, equation (22), requires knowing the initial wavenumber k_0, which is obtained from the waves' dispersion relation, equation (3b). The first term in that

equation, $\dot{\omega}|_{\text{disk}}$, is the rate at which the disk drives its own precession. The rate that a single annulus at a precesses due to the secular perturbations from another annulus at a' is

$$\delta\dot{\omega} = \frac{1}{na^2e}\frac{\partial(\delta R)}{\partial e}$$
$$= \frac{1}{2}\mu_d' n\alpha^{-1}\left[f(x') + g(x')\frac{e'(x')}{e}\cos(\tilde{\omega} - \tilde{\omega}')\right]dx', \quad (23)$$

where δR is equation (7). The total precession rate due to the disk's self-gravity is $\dot{\omega}|_{\text{disk}} = \int_{\text{disk}} \delta\dot{\omega}$, where the integration proceeds across the entire disk. Again, the integrand is a steep function of x' due to the softened Laplace coefficients that are present in the f and g functions, which allows us to replace the quantities $e'(x')$ and $\mu_d'(x')$ with the constants e and μ_d and to pull them out of the integral. And since $f(x') \simeq -g(x')$ when $|x'| \ll 1$ (from eqs. [5] and [10]),

$$\dot{\omega}|_{\text{disk}} \simeq \frac{1}{\pi}\mu_d n \int_{-x}^{\infty} \frac{x'^2 - 2\mathfrak{h}^2}{(x'^2 + 2\mathfrak{h}^2)^2}[1 - \cos(|k|ax')]dx' \quad (24a)$$

$$= \frac{2}{\pi}\mu_d n \int_{-x}^{\infty} \frac{x'^2 - 2\mathfrak{h}^2}{(x'^2 + 2\mathfrak{h}^2)^2}\sin^2\left(|k|\frac{ax'}{2}\right)dx' \quad (24b)$$

$$\equiv B_H'(|k|ax)|k|a\mu_d n, \quad (24c)$$

where

$$B_H'(z) = \frac{2}{\pi}\int_{-z}^{\infty}\frac{y^2 - H^2}{(y^2 + H^2)^2}\sin^2\left(\frac{y}{2}\right)dy. \quad (25)$$

When the disk is much thinner than the wavelength, $H = \sqrt{2}\mathfrak{h}|k|a \ll 1$, and

$$B_H'(z) \simeq \frac{1}{2} + \frac{1}{\pi}\text{Si}(z) + \frac{\cos z - 1}{\pi z}, \quad (26)$$

where $\text{Si}(z)$ is the sine integral of Abramowitz & Stegun (1972). In this limit, the $B_H'(z)$ function is identical to the $B_H(z)$ function of Hahn (2007) with both taking values of $1/2 < B_H' < 1$. And far downstream, where $z \to \infty$, the B_H' integral evaluates to

$$B_H'^{\infty} \equiv \lim_{z\to\infty} B_H'(z) = e^{-H} \quad (27)$$

for any value of H, which by the way, does differ a bit from the B_H function of Hahn (2007). The function $B_H'(z)$ is a dimensionless measure of the rate at which the disk drives its own precession, and this quantity becomes small when $H \gtrsim 1$, or when the disk thickness exceeds the wavelength. Evidently, a thick disk having $H \gg 1$ is less likely to sustain a density wave.

The satellite's gravity also precesses the planetary ring, at the rate

$$\dot{\omega}|_{\text{sat}} = \frac{1}{na^2e}\frac{\partial R_s}{\partial e} = \frac{1}{4}\mu_s n\left[f(\alpha) + g(\alpha)\frac{e_s}{e}\cos(\tilde{\omega} - \tilde{\omega}_s)\right] \quad (28)$$

$$\simeq \left[\frac{\mu_s}{2\pi(x+\Delta)^2} + \frac{\mu_d\sin(|k|ax)}{\pi|k|a(x+\Delta)^2}\right]n \quad (29)$$

when e_s/e is replaced with equation (22). The disturbing function associated with the central planet's oblateness is also

$$R_{\text{obl}} \simeq \frac{3}{4}J_2 e^2\left(\frac{R_p}{a}\right)^2(an)^2, \quad (30)$$

where J_2 is the planet's second zonal harmonic and R_p is the planet's radius (Murray & Dermott 1999), so precession due to oblateness is

$$\dot{\omega}|_{\text{obl}} = \frac{1}{na^2e}\frac{\partial R_{\text{obl}}}{\partial e} = \frac{3}{2}J_2\left(\frac{R_p}{a}\right)^2 n$$
$$\simeq \left[1 - \frac{7}{2}(x+\Delta)\right]\dot{\omega}_s|_{\text{obl}}, \quad (31)$$

where $\dot{\omega}_s|_{\text{obl}} \equiv (3J_2/2)(R_p/a_s)^2 n_s$ is the rate at which the satellite's orbit precesses due to oblateness, with n_s being the satellite's mean motion. Summing equations (24c), (29), and (31) then provides the dispersion relation for these spiral density waves,

$$\omega(|k|) \simeq D'(z)\mu_d|k|an + \frac{\mu_s n}{2\pi(x+\Delta)^2}$$
$$+ \left[1 - \frac{7}{2}(x+\Delta)\right]\dot{\omega}_s|_{\text{obl}}, \quad (32)$$

which is the angular rate at which the spiral density pattern rotates. The D' function in the above is

$$D'(z) = B_H'(z) + \frac{\sin z}{\pi(z + |k|a\Delta)^2}, \quad (33)$$

where $D'(z)$ is again numerically similar to the $D(z)$ function of Hahn (2007) which is also plotted in Figure 2 there, which shows that $D'(z)$ takes numerical values of $1/2 \leq D(z) \leq 1$ when $H \ll 1$.

2.2.1. Long and Short Density Waves

When these density waves have propagated far downstream of the satellite, the middle term in equation (32), which is the rate at which the satellite precesses the disk, becomes even more negligible with distance from the satellite, and the $D'(z)$ function becomes $D' \simeq B_H'^{\infty} = e^{-H}$, where $H = \sqrt{2}\mathfrak{h}|k|a$ should now be regarded as a dimensionless wavenumber. Thus, the downstream dispersion relation is

$$\omega(|k|) \simeq \mu_d|k|ane^{-\sqrt{2}\mathfrak{h}|k|a} + \dot{\omega}|_{\text{obl}}(x). \quad (34)$$

This dispersion relation can then be expressed in a more convenient dimensionless form via the combination

$$\omega^{\star} \equiv \frac{\sqrt{2}\mathfrak{h}}{\mu_d n}\left[\omega(|k|) - \dot{\omega}|_{\text{obl}}\right] = He^{-H}. \quad (35)$$

Figure 2 plots this dimensionless dispersion relation $\omega^{\star}$ versus the dimensionless wavenumber H, which shows that $\omega^{\star}$ has a maximum value of $\omega^{\star}_{\text{max}} = \exp(-1) \simeq 0.368$, which occurs for a wavenumber $H = 1$. This figure also shows that as long as the density wave's spiral pattern rotates at an angular rate $\omega^{\star} < \omega^{\star}_{\text{max}}$, then the disk can sustain two types of waves: long waves that have a wavenumber $H < 1$ and short waves that have $H > 1$, noting that these waves are called such since their wavelength is $\lambda = 2\pi/|k| = 2\sqrt{2}\pi h/H$. This upper limit on $\omega^{\star}$ also tells us that the disk can sustain these density waves when the spiral density pattern does not rotate too fast, namely, when (see also Hahn 2003)

$$\omega < \frac{\omega^{\star}_{\text{max}}\mu_d n}{\sqrt{2}\mathfrak{h}} + \dot{\omega}|_{\text{obl}}. \quad (36)$$
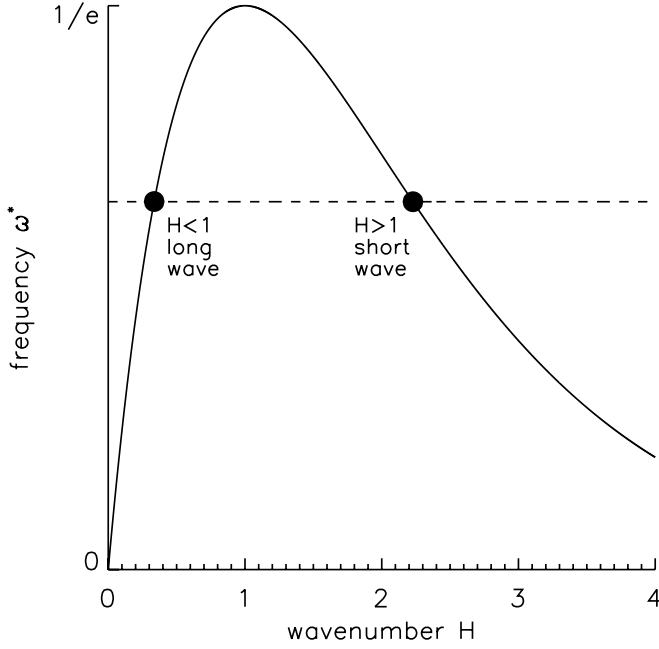
Fig. 2.—Dimensionless dispersion relation, eq. (35), plotted vs. the dimensionless wavenumber $H = \sqrt{2}\mathfrak{h}|k|a$. Note that $\omega^\star$ has a maximum value of $\omega^\star_{\max} = \exp(-1) \simeq 0.368$, which occurs when the wavenumber $H = 1$. When the spiral density pattern precesses at an angular rate $\omega^\star < \omega^\star_{\max}$, this dispersion relation has two solutions: a long-wavelength wave that has a wavenumber $H < 1$ and a short-wavelength wave that has a wavenumber $H > 1$.

2.2.2. Group Velocity

The waves' group velocity is $c_g = \partial\omega/\partial k$ (Toomre 1969; Shu 1984; Binney & Tremaine 1987), which becomes

$$c_g = s_k \frac{\partial\omega}{\partial|k|} = s_k(1-H)e^{-H}\mu_d an \qquad (37)$$

when the downstream dispersion relation is differentiated (eq. [34]); this is the rate of the spiral wave's radial propagation. Since the satellite is launching outward-propagating density waves from the disk's inner edge, $c_g > 0$, so equation (37) implies that the satellite can launch long $H < 1$ waves that have $s_k = \text{sgn}(k) = 1$ or short $H > 1$ waves that have $s_k = -1$. Spiral density waves having $k > 0$ are called trailing waves, since the more distant parts of a spiral arm trail in longitude, while leading waves have $k < 0$.

Section 2.2.4 will show that any waves excited by the Saturnian satellites Pan and Daphnis, both of which inhabit narrow gaps in Saturn's main A ring, would have a dimensionless wavenumber $H \ll 1$. This means that these satellites could launch long trailing waves that have $s_k = 1$ that would propagate outward at a rate $c_g \simeq \mu_d an$ (e.g., Hahn 2003). And since $\sin\phi_o = -s_k = -1$ (see § 2.1.2), then $\phi_o = -\pi/2$, which means that the longitude of periapse at the disk's inner edge would trail the satellite's longitude by $90°$.

Below, equation (47) will also show that the wavenumber $|k|$ and hence H will increase as the wave propagates downstream. So it is possible that a wave might travel far enough for the wavenumber H to increase beyond unity. If that happens, then equation (37) suggests three possible outcomes: the trailing wave can continue to advance further downstream with $c_g > 0$ as a short $(H > 1)$ leading $(s_k = -1)$ wave; or it can reflect $(c_g < 0)$ as a short $(H > 1)$ trailing $(s_k = +1)$ wave; or it might do both by spawning both types of wave trains. Note, however, that the

short wave would propagate at a substantially slower rate, $|c_g| \sim He^{-H}\mu_d an$, since $H > 1$. This site in the disk where $H = 1$ and c_g changes sign is a turning point for long waves. This site is also known as the Q-barrier, since its location depends on the value of Toomre's stability parameter $Q \simeq v_d n/\pi G\sigma = \mathfrak{h}/\mu_d$, where $v_d = hn$ is the particle disk's dispersion velocity (Toomre 1964).

2.2.3. Wavenumber and Wavelength

The wavenumber k is obtained after calculating the satellite's precession rate $\dot{\tilde{\omega}}_s$. When the system is in steady state, both the satellite and the spiral wave precess at the same rate, $\dot{\tilde{\omega}}_s = \omega(|k|)$, which then provides a simple relation for k that depends only on the system's physical constants, namely, μ_d, Δ, and J_2.

The satellite's longitude of periapse $\tilde{\omega}_s$ precesses due to perturbations from the disk and the central planet oblateness, with this precession occurring at the rate

$$\dot{\tilde{\omega}}_s = \dot{\tilde{\omega}}_s\big|_{\text{disk}} + \dot{\tilde{\omega}}_s\big|_{\text{obl}}, \qquad (38)$$

where $\dot{\tilde{\omega}}_s\big|_{\text{disk}} = \int_{\text{disk}}\delta\dot{\tilde{\omega}}_s$ is the satellite's precession rate due to the entire disk, where

$$\delta\dot{\tilde{\omega}}_s = -\frac{1}{2}\mu_d' n_s \frac{g(\alpha)}{\alpha}\left[1 - \frac{e'}{e_s}\cos(\tilde{\omega}_s - \tilde{\omega}')\right]dx' \qquad (39)$$

is the satellite's precession rate due to a disk annulus of radius a' and mass $\delta m'$. This is obtained from equation (23) when n, a, e, and $\tilde{\omega}$ are replaced with n_s, a_s, e_s, and $\tilde{\omega}_s$, and the separation $x' \rightarrow x' + \Delta$. The satellite's precession rate due to the entire disk is

$$\dot{\tilde{\omega}}_s\big|_{\text{disk}} = \int_{\text{disk}}\delta\dot{\tilde{\omega}}_s$$

$$\simeq \frac{1}{\pi}\mu_d n_s \int_0^\infty (x'+\Delta)^{-2}\left[1 - \frac{e}{e_s}\cos(kax' - \phi_o)\right]dx' \qquad (40a)$$

$$\simeq \frac{\mu_d n_s}{\pi\Delta} + \frac{\mu_s n_s}{2\pi\Delta^2}S(|k_0|a\Delta), \qquad (40b)$$

where

$$S(|k_0|a\Delta) \equiv |k_0 a\Delta|^2 \int_0^\infty \frac{\sin(y)dy}{(y + |k_0|a\Delta)^2} \qquad (41)$$

is another dimensionless function that depends on the initial wavenumber $|k_0|$ and the gap width Δ. This quantity is also plotted in Figure 2 of Hahn (2007) which shows that S takes numerical values of $0 \leq S(|k_0|a\Delta) \leq 1$.

The first term in equation (40b) is the rate at which the undisturbed disk precesses the satellite's orbit, while the second term is the additional precession that the satellite experiences due to the density wave in the disk. Note, however, that if the satellite instead orbited at the center of a narrow gap in the disk, then the first term in equation (40b) would be doubled due to the disk matter orbiting interior to the satellite. One would also expect additional precession to occur due to any density waves that might be launched in this interior disk. However, it will be shown below that this contribution is unimportant. With this in mind, equation (40b) is generalized to account for a possible inner disk by writing

$$\dot{\tilde{\omega}}_s\big|_{\text{disk}} \simeq \frac{\varepsilon\mu_d n_s}{\pi\Delta} + \frac{\mu_s n_s}{2\pi\Delta^2}S(|k_0|a\Delta), \qquad (42)$$

where $\varepsilon = 1$ if the disk lies entirely interior or exterior to the satellite and $\varepsilon = 2$ if the satellite instead orbits in the center of a gap whose fractional half-width is Δ. The satellite's total precession rate then becomes

$$\dot{\omega}_s = \dot{\omega}_s|_{\text{disk}} + \dot{\omega}_s|_{\text{obl}} = \frac{\varepsilon \mu_d n_s}{\pi \Delta} + \frac{\mu_s n_s}{2\pi \Delta^2} S(|k_0|a\Delta) + \dot{\omega}_s|_{\text{obl}}. \tag{43}$$

When the disk and satellite are in steady state, the satellite and its spiral wave pattern both precess in concert, so $\dot{\omega}_s = \omega(|k|)$, which becomes

$$\pi D'(z)|k|a\Delta = \varepsilon + \frac{\mu_c}{\mu_d}\left(1 + \frac{x}{\Delta}\right) + \frac{\mu_s}{2\mu_d\Delta}f(|k_0 a\Delta|, z), \tag{44}$$

where

$$f(|k_0 a\Delta|, z) = S(|k_0|a\Delta) - \frac{|k_0 a\Delta|^2}{(|k_0 a\Delta| + z)^2} \tag{45}$$

is another function that takes values of $-1 \leq f \leq 1$, and

$$\mu_c \equiv \frac{21\pi}{4}\left(\frac{R_p\Delta}{a_s}\right)^2 J_2 \tag{46}$$

is called the critical disk mass (Hahn 2007).

Two additional assumptions will then provide a simple expression for the wavenumber k. First, assume that the right term in equation (44) is small compared to the middle term, which requires the satellite's mass to be sufficiently small, namely, that $\mu_s \ll 2\mu_c\Delta$. Second, assume that the dimensionless wavenumber obeys $H \ll 1$, which means that $D'(z) \to 1$ downstream. Note, however, that $D'(z)$ is not unity in the wave launch zone; rather, it takes values of $1/2 \leq D'(z) \leq 1$ over the initial wavelength (see Fig. 2 of Hahn 2007). However, a sufficiently accurate result is obtained when $D'(z)$ is replaced with its average value over the first wavelength, $\bar{D} \simeq 0.87$ (Hahn 2007). These assumptions will be confirmed below in § 2.2.4. With these assumptions in hand, equation (44) then yields the wavenumber

$$|k(x)| \simeq \frac{1}{\pi\bar{D}a\Delta}\left[\varepsilon + \frac{\mu_c}{\mu_d}\left(1 + \frac{x}{\Delta}\right)\right], \tag{47}$$

with

$$|k_0| = \frac{\varepsilon + \mu_c/\mu_d}{\pi\bar{D}a\Delta} \tag{48}$$

being the initial wavenumber evaluated at $x = 0$.

The first wavelength λ_0 is obtained from $\int_0^{\lambda_0} |k|da = 2\pi$. When $\mu_c \ll \mu_d$, that integral yields

$$\lambda_0 \simeq 2\pi^2 \bar{D}a\Delta/\varepsilon. \tag{49}$$

However, when $\mu_c \gtrsim \mu_d$ (which occurs when the central planet is too oblate or the disk mass is too small), the wavenumber k varies with distance x, which violates a key assumption in the derivation of the wave amplitude (§ 2.1.1). The numerical experiment described in § 4.3 will also show that the wave amplitude (eq. [52], derived below) is smaller than expected in this case. Nonetheless, that experiment also shows that the formula for the expected wavenumber, equation (47), is quite reliable when $\mu_c \gtrsim \mu_d$.

2.2.4. Checking the Assumptions

These results will be applied to the Saturnian satellites Pan and Daphnis that orbit in narrow gaps in Saturn's main A ring. Pan has a mass $\mu_s = 8.7 \times 10^{-12}$ Saturn masses (Porco et al. 2007) and a semimajor axis $a_s = 133,584$ km (Jacobson et al. 2008). Pan orbits near the center of the Encke gap whose half-width is $\Delta a = 162.5$ km (Porco et al. 2005), so its fractional half-width is $\Delta = \Delta a/a_s = 0.0012$. Saturn's radius is $R_p = 60,330$ km and its second zonal harmonic is $J_2 = 0.0163$, so the critical disk mass is $\mu_c = 7.9 \times 10^{-8}$. Consequently, the quantity $2\mu_c\Delta = 1.9 \times 10^{-10}$, which does indeed satisfy the requirement that $\mu_s \ll 2\mu_c\Delta$.

This same assumption is also satisfied by Daphnis, whose mass is $\mu_s = 1.5 \times 10^{-13}$ (Porco et al. 2007), but by a smaller margin. Daphnis orbits in the Keeler gap, which itself is about 2900 km beyond the Encke gap. The Keeler gap is also about 8 times narrower than the Encke gap (Tiscareno et al. 2005), so $\Delta \simeq 1.5 \times 10^{-4}$, which reduces the critical disk mass to $\mu_c \simeq 1.2 \times 10^{-9}$. Consequently, $\mu_s < 2\mu_c\Delta$ is still satisfied, but only by a factor of ~2.5.

The other requirement is that $H = \sqrt{2}\mathfrak{h}|k|a \ll 1$. The ring's vertical thickness is about $h \simeq 30$ m near the Encke gap (Tiscareno et al. 2007), so the ring's fractional thickness is $\mathfrak{h} = h/a_s \simeq 2 \times 10^{-7}$; a comparable thickness can also be inferred from the A ring viscosity that is reported in Porco et al. (2007). The ring's surface density here is $\sigma \simeq 46$ g cm^{-2} (Tiscareno et al. 2007), so the normalized disk mass is $\mu_d = \pi\sigma a_s^2/M \simeq 4.5 \times 10^{-8}$, which means that Pan's initial wavenumber is $|k_0|a \simeq 1100$ by equation (48), while Daphnis has $|k_0|a \simeq 5000$. Consequently, $H = \sqrt{2}\mathfrak{h}|k|a \sim O(10^{-3} \text{ to } 10^{-4}) \ll 1$ is very well satisfied. And since $H < 1$, this means that these satellites will launch long trailing density waves that propagate radially outward from the gap edge, provided these satellites have nonzero eccentricities.

2.2.5. Waves in an Interior Disk

A satellite that orbits in the center of a gap in a broad planetary ring might also excite a disturbance in the disk material that orbits interior to the satellite. The dispersion relation for any density waves launched at the inner gap edge is

$$|k(x)| \simeq \frac{1}{\pi\bar{D}a|\Delta|}\left[\varepsilon - \frac{\mu_c}{\mu_d}\left(1 + \left|\frac{x}{\Delta}\right|\right)\right], \tag{50}$$

which may be derived via the method that is described in footnote 1 of Hahn (2007). This dispersion relation is identical to equation (47) except for the sign on the term that is proportional to the critical mass. Since the right-hand side of equation (50) must be positive wherever the wave propagates, this equation tells us that these density waves are only allowed inward a distance $|x| < x_{\text{in}}$, where

$$x_{\text{in}} \equiv \left(\frac{\varepsilon\mu_d}{\mu_c} - 1\right)|\Delta| \tag{51}$$

is the distance of the waves' maximum inward excursion. For Pan, this distance evaluates to $x_{\text{in}} \simeq 0.1\Delta$, which corresponds to a physical distance of $x_{\text{in}}a_s \simeq 15$ km, which is only a tiny fraction of the wave's initial wavelength that is calculated below in § 2.3. In short, the A ring material that orbits interior to Pan is unable to sustain this type of density wave.

Note, however, that x_{in} is a bit larger for the ring material that orbits interior to Daphnis and the Keeler gap. However, Daphnis's small mass (Porco et al. 2007) and low eccentricity (Jacobson

et al. 2008) results in waves of such low amplitude that this issue is moot.

2.3. Wave Amplitude, Continued

Plugging the initial wavenumber, equation (48), into equation (22) then yields an expression for the amplitude of the density wave that is now written only in terms of the system's known physical parameters,

$$\frac{e}{e_s} \simeq \frac{\mu_s(\varepsilon + \mu_c/\mu_d)}{2\pi\bar{D}\mu_d\Delta}. \tag{52}$$

However, keep in mind that this derivation requires that the wavelength vary little over the first wavelength, which in turn requires $\mu_c \ll \mu_d$. The simulations described in § 4.3 show that equation (52) overestimates the wave amplitude when $\mu_c \gtrsim \mu_d$.

Pan's eccentricity is $e_s = 1.4 \times 10^{-5}$ (Jacobson et al. 2008), so equation (52) predicts eccentricities of $e \sim 1.5 \times 10^{-6}$ due to the density wave that Pan excites at the outer edge of the Encke gap, since $\varepsilon = 2$, $\mu_c = 7.9 \times 10^{-8}$, and $\mu_d \simeq 4.5 \times 10^{-8}$ (see § 2.2.4). However, this is actually an overestimate, since $\mu_c/\mu_d \simeq 1.8$ is not small, which is a key assumption in the derivation of equation (52). In fact, the simulation described in § 4.3 shows that equation (52) overestimates the amplitude of Pan's waves by a factor of $\gamma \simeq 4$, so the epicyclic amplitude due to this wave at the outer Encke gap is only $\Delta r = ea_s/\gamma \sim 50$ m, which is likely too small to be seen by a spacecraft such as *Cassini*. And since this wave's initial wavenumber is $|k_0|a \simeq 1100$ (§ 2.2.4), its initial wavelength would be $\lambda_0 = 2\pi/|k_0| \simeq 760$ km, which is also far longer than the wavelengths of any of the more familiar density waves that satellites routinely launch at their many mean-motion resonances in the rings.

Recall that the wavenumber $|k|$ increases with distance x (see eq. [47]), so the wavelength λ shrinks as the wave propagates outward. Note that the A ring's outer edge is $\Delta a \simeq 3200$ km away from the Encke gap, which corresponds to a fractional distance of $x = \Delta a/a_s \simeq 0.024$. Inserting this into equation (47) then yields a wavenumber of $|k|a \simeq 1.2 \times 10^4$, which corresponds to a wavelength of $\lambda_0 = 2\pi/|k_0| \simeq 70$ km when the wave hits the outer edge of the A ring. This presumes that the wave was not damped en route by the ring's viscosity, but § 2.3.1 shows that the viscous damping of these long outbound waves is modest. The reflection of these undamped waves near the outer edge of the A ring is also discussed in § 4.2.

The fractional variation in the disk's surface density due to the density wave is (Borderies et al. 1985; Hahn 2003)

$$\frac{\Delta\sigma}{\sigma_0} \simeq \frac{\partial(ea)}{\partial a} \cos(\theta - \tilde{\omega}) + ea\frac{\partial\tilde{\omega}}{\partial a} \sin(\theta - \tilde{\omega}), \tag{53}$$

where θ is the longitude in the disk and σ_0 is the surface density of the undisturbed disk. The first term is negligible since the downstream eccentricity e is constant, so the magnitude of the fractional variation in surface density variations due to the wave is dominated by the second term, which is

$$\left|\frac{\Delta\sigma}{\sigma_0}\right| \simeq ea|k| \tag{54}$$

since $k = -\partial\tilde{\omega}/\partial a$ (see eq. [13]). Since the wave launched by Pan has an amplitude of $e \sim 4 \times 10^{-7}$ and an initial wavenumber of $|k_0|a \simeq 1100$, the surface density variations due to this wave are quite small, only $\Delta\sigma/\sigma_0 \simeq ea|k| \sim 4 \times 10^{-4}$, which again is too small for detection. However, it might be easier to see this

wave further downstream, due to the increase in $|k|$ with distance x. For instance, $|k|$ will have increased by a factor of 10 when the wave reaches the outer part of the A ring, so $\Delta\sigma/\sigma \sim 4 \times 10^{-3}$ there, but this again is probably still too small for detection. Thus, the observational consequences of these density waves are seemingly slight. Nonetheless, these waves are not totally inconsequential, since § 3 will show that the excitation of these waves can also result in a vigorous damping of the satellite's eccentricity.

2.3.1. Viscous Damping of Spiral Density Waves

The variations in the ring's surface density due to the density wave are dominated by the second term in equation (53), so $\Delta\sigma \simeq -\sigma_0 eka \sin(\theta - \tilde{\omega})$, where the ring's longitude of periapse is $\tilde{\omega}(a, t) = \omega t - \int^a k(r)dr$, with the ωt term accounting for the spiral pattern's rotation with time due to the system's precession. Inserting this into the above shows that $\Delta\sigma$ has the form $\Delta\sigma = \text{Re}(Se^{i\phi})$, which has an amplitude $|S(a)| = \sigma_0 e|k|a$ and a phase

$$\phi(a, \theta, t) = m\theta - \omega t + \int^a k(r)dr, \tag{55}$$

noting that θ in the above was multiplied by $m = 1$ so that this work is readily compared to other studies of density waves developed for spiral patterns having $m \geq 1$ arms.

When there is no dissipation in the system, the wavenumber k in equation (55) is real (e.g., eq. [47]). However, if there is any dissipation in the disk, then the wavenumber k acquires an imaginary component, i.e., $k \to k_R + ik_I$, which causes exponential damping of the wave's amplitude. If that dissipation is due to the disk's kinematic viscosity ν, then the imaginary part of the wavenumber is[1] (Shu 1984)

$$k_I = \frac{\nu k_R^3}{mn - \omega} + \frac{7s_k\nu k_R^2(mn - \omega)}{6\pi G\sigma_0} \simeq \frac{\nu k_R^3}{n}\left(1 + \frac{7}{6\mu_d|k_R|a}\right), \tag{56}$$

where k_R is the real part of the wavenumber (eq. [47]), $s_k = \text{sgn}(k_R) = +1$, $m = 1$, and noting that $\pi G\sigma_0 = \mu_d an^2$ and that the spiral pattern rotates slowly, i.e., $\omega \ll n$. Since the long waves launched by Pan have wavenumbers of $|k|a \sim 10^3$-10^4 (see § 2.3) and the A ring's normalized disk mass is $\mu_d \simeq 4.5 \times 10^{-8}$ (§ 2.2.4), it is clear that the second term in equation (56) dominates over the first, so

$$k_Ia \simeq \frac{7}{6\mu_d}\left(\frac{\nu}{a^2n}\right)|k_Ra|^2 \tag{57}$$

for outward-propagating long waves. Consequently, the ring's surface density varies as

$$\Delta\sigma = \text{Re}(Se^{i\phi}) \propto \exp\left[-\int_0^x k_I(r)dr\right], \tag{58}$$

which reveals how ring viscosity reduces the amplitude of the wave as it travels a fractional distance x.

---

[1] Comparison of eq. (55) to the phase convention adopted in Shu (1984) shows that the signs of m and ω are reversed. This sign reversal is accounted for in eq. (56).

It is anticipated that the wave's viscous damping length ℓ_ν will be much larger than the gap half-width Δ. In that case, the wavenumber that appears in the above formulae is approximately

$$|k_R|a \simeq \frac{\mu_c x'}{\pi \bar{D} \mu_d \Delta^2} \qquad (59)$$

by equation (47). Inserting this into equation (57) and then evaluating the integral in equation (58) shows that

$$\Delta\sigma \propto e^{-(x/\ell_\nu)^3}, \qquad (60)$$

where ℓ_ν is the viscous damping length in units of a_s,

$$\ell_\nu = \left[\left(\frac{18\mu_d^3}{7} \right) \left(\frac{a^2 n}{\nu} \right) \left(\frac{\pi \bar{D} \Delta^2}{\mu_c} \right)^2 \right]^{1/3}. \qquad (61)$$

The following evaluates this viscous damping length ℓ_ν for the waves that Pan would launch at the outer edge of the Encke gap.

There are two sources of viscosity in Saturn's rings: collisions among ring particles, and gravitational wakes. Viscosity due to collisions among ring particles is $\nu_c \simeq 0.46c^2\tau/n(1 + \tau^2)$, where $c = hn$ is the particle's dispersion velocity and τ is the ring optical depth (Goldreich & Tremaine 1982). Thus, the dimensionless viscosity combination $\nu_c/a^2 n$ in the above evaluates to

$$\frac{\nu_c}{a^2 n} \simeq \frac{0.46 \mathfrak{h}^2 \tau}{1 + \tau^2} \simeq 8 \times 10^{-15}, \qquad (62)$$

since the outer A ring has an optical depth of $\tau \simeq 0.6$ and $\mathfrak{h} \simeq 2 \times 10^{-7}$. Note that the viscosity that is associated with the ring's gravitational wakes ν_g is also comparable, since

$$\frac{\nu_g}{a^2 n} = \frac{CG^2\sigma^2}{a^2 n^4} = \frac{C\mu_d^2}{\pi^2} \simeq 7 \times 10^{-15}, \qquad (63)$$

where the coefficient $C \simeq 33$ for the A ring (Daisaka et al. 2001) and $\mu_d \simeq 4.5 \times 10^{-8}$. This all suggests that the total viscosity in the outer A ring is around $\nu/a^2 n \sim 10^{-14}$. Inserting this into equation (61) then shows that the viscous damping length for Pan's waves (with $\Delta = 0.0012$ and $\mu_c = 7.9 \times 10^{-8}$) is $\ell_\nu \simeq 0.039$, which corresponds to a physical distance of $\ell_\nu a_s \simeq 5200$ km. Note, however, that the outer edge of the A ring only lies at a fractional distance of $x \simeq 0.024$, which means that the amplitude of Pan's outbound density waves is reduced only by a factor of $e^{-(x/\ell_\nu)^3} \simeq 0.8$ as it travels across the A ring. This calculation indicates that the damping of long waves due to ring viscosity is only of marginal importance.

Section 4.3 also shows that this long wave will reflect at the outer edge of the A ring (or else at the nearby Keeler gap) and march back toward Pan as a superposition of both long and short waves that are of roughly equal magnitudes. Pan's outbound long density waves will have a dimensionless wavenumber $H_L = \sqrt{2\mathfrak{h}}|k|a \simeq 3.4 \times 10^{-3} \ll 1$ when they near the outer edge of the A ring. Let H_S be the dimensionless wavenumber of the reflected short waves. Since the long and short spiral wave patterns both precess at the same rate, the wavenumbers H_L and H_S both satisfy the same dimensionless dispersion relation, equation (35), so

$$H_L \simeq \omega^\star = H_S e^{-H_S}. \qquad (64)$$

This is solved numerically for the wavenumber of the reflected short wave, $H_S \simeq 7.7$, which yields a physical wavenumber of

$|k_s|a \simeq 2.7 \times 10^7$, since $\mathfrak{h} \simeq 2 \times 10^{-7}$. This corresponds to a wavelength $\lambda_s = 2\pi/|k_s|$ that is comparable to the disk's scale height $h = \mathfrak{h}a_s \sim 30$ m. These very short wavelength waves will be nonlinear ($\Delta\sigma/\sigma > 1$), and they will likely damp on a very short spatial scale.

3. DAMPING THE SATELLITE'S ECCENTRICITY

The excitation of these density waves also alters the satellite's eccentricity e_s at a rate that can be calculated from the angular momentum flux that is transported by these waves. The angular momentum content of a narrow annulus in the disk is $\delta L = \delta m[GMa(1 - e^2)]^{1/2}$, where $\delta m = \sigma \delta A$ is the mass of that annulus which has an area δA and a mass surface density σ. The surface density of angular momentum in that annulus is then $\ell = \delta L/\delta A = \sigma na^2(1 - e^2)^{1/2} \simeq \sigma na^2(1 - e^2/2) = \ell_0 + \ell_w$, where $\ell_0 = \sigma na^2$ would be the angular momentum surface density if the ring were circular, and $\ell_w = -\sigma e^2 na^2/2$ is the surface density of angular momentum that is associated with the wave whose amplitude is e. The flux of angular momentum that is transported by the wave is $F = \ell_w c_g$, where $c_g = \mu_d an$ is the group velocity of long density waves (see § 2.2.2). Consequently, the angular momentum luminosity, which is the rate at which waves transport angular momentum across an annulus of radius a, is $\mathcal{L} = 2\pi aF = -(e\mu_d an)^2 M$.

Note the sign on $\mathcal{L}$, which means that these waves transport angular momentum inward, from the disk to the satellite. This transport also increases the satellite's angular momentum $L_s = m_s[GMa_s(1 - e_s^2)]^{1/2} \simeq m_s n_s a_s^2(1 - e_s^2/2)$ at the rate $dL_s/dt \simeq -m_s n_s a_s^2 e_s \dot{e}_s = -\mathcal{L}$, which then provides the rate at which wave excitation tends to damp the satellite's eccentricity,

$$\dot{e}_s = -\frac{e^2 \mu_d^2}{e_s \mu_s} n_s. \qquad (65)$$

And if the wavenumber varies little over that first wavelength, which requires $\mu_c \ll \mu_d$, then the wave amplitude e is given by equation (52), which yields the satellite's eccentricity damping rate

$$\frac{\dot{e}_s}{e_s} = -\frac{\mu_s(\varepsilon + \mu_c/\mu_d)^2}{(2\pi \bar{D}\Delta)^2} n_s \qquad (66)$$

and the eccentricity decay timescale

$$\tau_e = \left| \frac{e_s}{\dot{e}_s} \right| = \frac{2\pi(\bar{D}\Delta)^2}{\mu_s(\varepsilon + \mu_c/\mu_d)^2} P_{\text{orb}}, \qquad (67)$$

where $P_{\text{orb}} = 2\pi/n_s$ is the satellite's orbit period.

If, however, $\mu_c \gtrsim \mu_d$, then equation (52) will overestimate the wave amplitude e, and equation (66) will not be valid. Nonetheless, equation (65) can still be used to determine the satellite's e-damping rate, but the wave amplitude e must be determined by other means, such as by using the rings model that is described in § 4.

3.1. Comparison to Lindblad and Corotation Resonances

The satellite is also perturbing the planetary ring at its many Lindblad and corotation resonances in the disk, and this interaction also causes the satellite's eccentricity to evolve at the rate

$$\dot{e}_s|_{\text{L,cor}} = \dot{e}_s|_{\text{L}} + \dot{e}_s|_{\text{cor}}, \qquad (68)$$

where the first term represents the eccentricity excitation that is due to the Lindblad resonances and the second term is the

eccentricity damping that is due to corotation resonances. The rate at which the satellite's eccentricity e_s evolves due to its Lindblad resonances in a narrow annulus of mass $\delta m'$ that lies a fractional distance x' away is (from Goldreich & Tremaine 1981)

$$\delta \dot{e}_s|_{\rm L} = \frac{f_{\rm L} \mu_s e_s}{2|x'|^5} \frac{\delta m'}{M} n_s, \tag{69}$$

where the factor $f_{\rm L} \simeq 3.045$. The satellite's total eccentricity variation due to all of its Lindblad resonances throughout the disk is obtained by setting $\delta m' = 2\pi \sigma' a' \, da' = 2\mu_d' M \, dx'$ and integrating equation (69) across the disk, which yields

$$\dot{e}_s|_{\rm L} = 2 \int_{\Delta}^{\infty} \delta \dot{e}_s|_{\rm L} = \frac{f_{\rm L} \mu_s \mu_d e_s}{2\Delta^4} n_s, \tag{70}$$

where the factor of 2 in the middle term accounts for the ring material orbiting interior and exterior to the satellite. The e-excitation timescale due to Lindblad resonances is then

$$\tau_{\rm L} = \frac{e_s}{\dot{e}_s|_{\rm L}} = \frac{\Delta^4}{\pi f_{\rm L} \mu_s \mu_d} P_{\rm orb}. \tag{71}$$

The satellite also has many corotation resonances that lie in the planetary ring, and their effect is to damp the satellite's eccentricity at a rate $\dot{e}_s|_{\rm cor}$ that has the same form as equations. (69)–(70) but with a lead coefficient of $f_{\rm cor} = -3.193$ (Goldreich & Tremaine 1981). However, this eccentricity damping only occurs if the particles' motions at the corotation resonances are not saturated. The total rate at which the satellite's eccentricity varies due to its Lindblad and corotation resonances is

$$\dot{e}_s|_{\rm L,cor} = \dot{e}_s|_{\rm L} + \dot{e}_s|_{\rm cor} = \frac{f_{\rm L,cor} \mu_s \mu_d e_s}{2\Delta^4} n_s, \tag{72}$$

where the factor $f_{\rm L,cor} = f_{\rm L} + f_{\rm cor} = -0.148$, which indicates that the net effect of these resonances is to damp the satellite's eccentricity, provided the corotation resonances are not saturated. Note, however, that $|f_{\rm L,cor}/f_{\rm L}| \simeq 5\%$, which means that eccentricity damping wins by only a small margin. Consequently, the total e-damping timescale due to Lindblad and corotation resonances is then

$$\tau_{\rm L,cor} = \left| \frac{e_s}{\dot{e}_s|_{\rm L,cor}} \right| = \frac{\Delta^4}{\pi |f_{\rm L,cor}| \mu_s \mu_d} P_{\rm orb}. \tag{73}$$

If, however, the corotation resonances are saturated, then the Lindblad resonances will pump up the satellite's eccentricity, but at a rate that is half of equation (70) (see Goldreich & Tremaine 1981). Nonetheless, the satellite's secular perturbations of the ring will also endeavor to damp the satellite's eccentricity at the rate given by equation (66). Comparing these two rates will show that eccentricity damping is still assured when the satellite's gap is sufficiently wide,

$$\Delta^2 > f_{\rm L} (\pi \bar{D})^2 \mu_d / 2, \tag{74}$$

provided $\mu_c \ll \mu_d$.

Daphnis satisfies the $\mu_c \ll \mu_d$ condition, and since $\mu_d \simeq 4.5 \times 10^{-8}$, $\bar{D} = 0.87$, and $\varepsilon = 2$, the above gap-width requirement evaluates to $\Delta \gtrsim 7 \times 10^{-4}$. However, the Keeler gap's half-

width is only $\Delta \simeq 1.5 \times 10^{-4}$, so this requirement is not satisfied. Consequently, if Daphnis's corotation resonances were in fact saturated, then this secular e-damping could not counterbalance the effects of the Lindblad resonances, which would pump up Daphnis's eccentricity until that satellite crashed into the A ring. That Daphnis has a very low eccentricity suggests that the motions of the ring particles at its corotation resonances are not saturated.

Note that Pan does not satisfy $\mu_c \ll \mu_d$, so equation (74) does not apply to this satellite. Instead, the rings model of § 4.3 is used to assess that satellite's e-damping rate.

4. SIMULATIONS OF DENSITY WAVES LAUNCHED AT A GAP EDGE

The rings model of Hahn (2003) is used to test the preceding results. This model treats the disk as a set of N discrete gravitating annuli having semimajor axes a_j, eccentricities e_j, longitudes of periapse $\tilde{\omega}_j$, and half-thicknesses h_j. The model only considers the system's secular gravitational perturbations, so it also solves the same equations of motion, equations (1), but it does so without making any of the approximations and assumptions invoked in § 2. Consequently, the model provides another check on the analytic results obtained above.

4.1. Outbound Waves

The rings model is used to simulate the spiral density waves that are launched by an eccentric satellite that orbits just interior to a disk. Figure 3 shows the amplitude of this wave as it advances across a disk, with the system's parameters being detailed in the figure caption. Note, however, that those parameters do not correspond to any real ring-satellite system. Rather, these parameters were chosen to illustrate the results of § 2 in the limit in which those results were obtained, namely, that the factor μ_c/μ_d appearing in the wavenumber equation (47) is modest, with $\mu_c/\mu_d = 0.2$. This causes the wavenumber to vary only a small amount across the first wavelength, which is a key assumption of § 2.1's derivation of the wave amplitude. Nonetheless, the simulation reported in Figure 3 does correspond loosely to a small ~ 10 km satellite orbiting just interior to a ring whose surface density is similar to Saturn's main A ring.

The amplitude of the simulated wave compares favorably with the wave's expected amplitude, equation (52), which is indicated by the dashed line in Figure 3. The wave propagation time also provides another check on these calculations. Note that the time for these waves to propagate a fractional radial distance $x = \Delta r/a$ is

$$t_{\rm prop} = \frac{\Delta r}{c_g} = \frac{x P_{\rm orb}}{2\pi \mu_d}, \tag{75}$$

where c_g is the waves' group velocity, equation (37). The simulated disk has a normalized mass of $\mu_d = 5 \times 10^{-8}$ and a fractional width $x = 0.015$, so the anticipated propagation time is $t_{\rm prop} = 48 \times 10^3$ orbits, which compares well with the simulated wave's propagation time (Fig. 3).

Section 2.2.2 predicts that the satellite will launch a long trailing density wave that has $s_k = \mathrm{sgn}(k) = +1$. So by equation (13), this means that the disk's longitude of periapse $\tilde{\omega}(a)$ should steadily decrease at greater distances a in the disk. This is confirmed in Figure 4, which shows the waves' longitudes relative to the satellite's, $\tilde{\omega}(a) - \tilde{\omega}_s$. Also note that the longitude of periapse at the disk's inner edge is $90°$ behind the satellite's longitude, as expected. We find that once the density wave is established in the disk, its longitudes $\tilde{\omega}(a)$ precess at the same
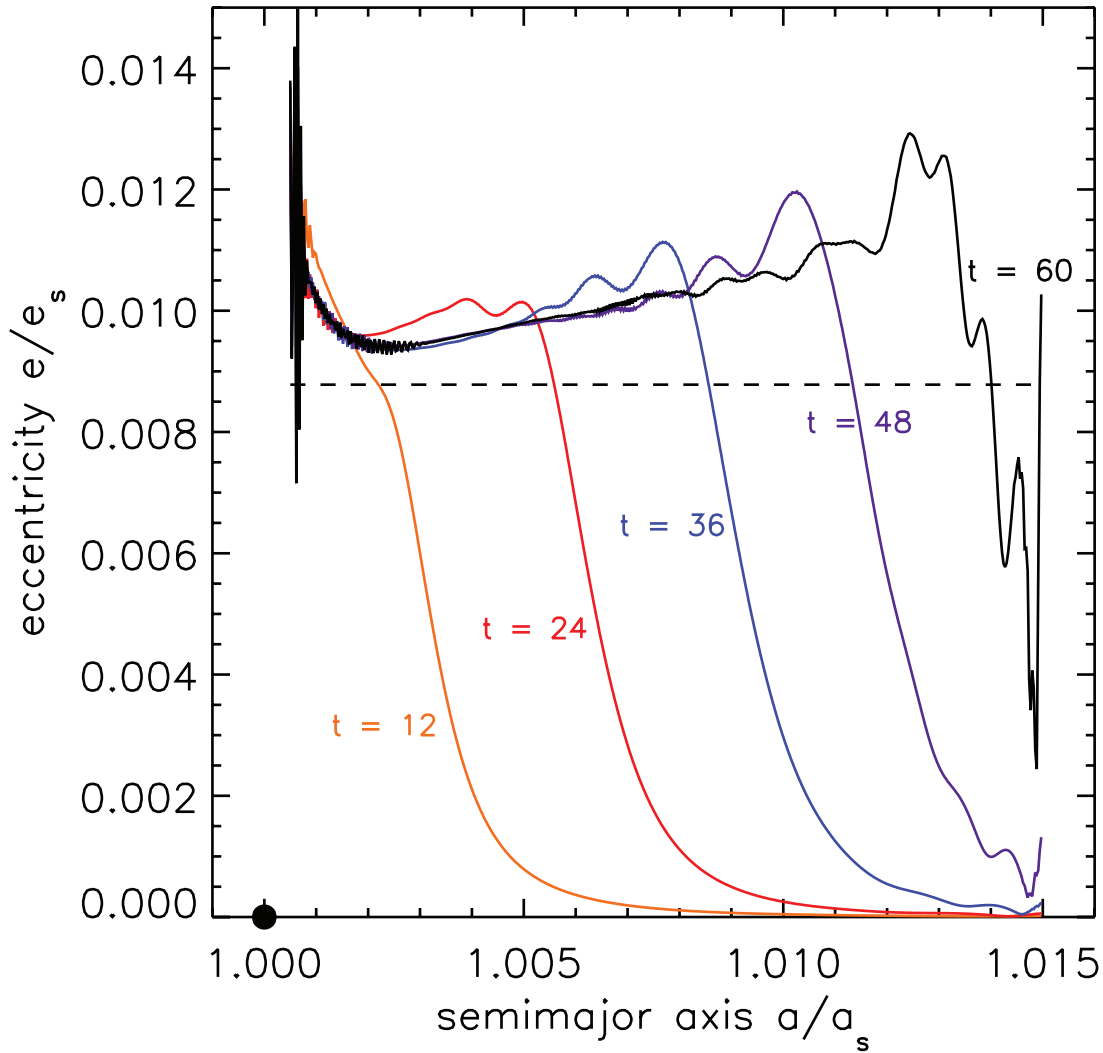
FIG. 3.—Rings model used to simulate spiral density waves launched by an eccentric satellite that orbits just interior to a disk. The satellite's normalized mass is $\mu_s = 10^{-12}$, and the disk is comprised of $N = 500$ rings having semimajor axes distributed over $1 + \Delta \leq a_j/a_s \leq 1.015$, where $\Delta = 5 \times 10^{-4}$ is the fractional distance between the satellite and the innermost ring. The rings' fractional masses are $\mu_r = 2.9 \times 10^{-12}$, so the normalized disk mass is $\mu_d = \pi \sigma r^2/M = (\mu_r/2)(a_s/\delta) = 5 \times 10^{-8}$, where the rings' fractional separations are $\delta/a_s = 0.0145/N = 2.9 \times 10^{-5}$. The rings' fractional half-widths $\mathfrak{h}$ are also set equal to their separations δ/a_s. The central planet's zonal harmonic is $J_2 = 0.012$, and the planet's radius is $R_p/a_s = 0.45$, so this system's critical disk mass is $\mu_c = 1.0 \times 10^{-8}$ and $\mu_c/\mu_d = 0.2$. The satellite's initial eccentricity is $e_s = 10^{-5}$, with all other rings initially having zero eccentricities. The curves show the fractional amplitude of the density wave, $e(a)/e_s$, as it advances across the disk, shown at selected times t in units of 10^3 orbital periods. The dashed line is the expected wave amplitude, eq. (52), with $\varepsilon = 1$.

rate as the satellite's, and that the disk's eccentricities $e(a)$ are also constant, which confirms the steady state assumption employed in equations (3). The disk's surface density variations due to the wave are given in equation (53), which is dominated by the second term. Inspection of that term shows that the disk's maximum surface density occurs at longitudes that trail those shown in Figure 4 by 90°, while the disk's minimum surface density (Fig. 4) leads by 90°.

Figure 4 also plots the dimensionless wavenumber $|k|a\Delta$ across the disk at time $t = 60 \times 10^3$ orbits, when the density wave just starts to reflect at the disk's outer edge. Also plotted is the expected wavenumber, equation (47), which compares well. The simulation's variations in k at the disk's far edge are due to the wave reflecting there, while the variations near the disk's inner edge are due to the very short wavelength variations in $\tilde{\omega}(a)$ that are just barely seen in the top panel. Those wiggles are the short waves that are described in § 2.2.2. Evidently, the satellite also launches short-wavelength leading waves at the disk's inner edge, which are the cause for the high-frequency wiggles also seen in the $t = 60$ curve shown in Figure 3. Figure 4 also shows

that the short waves propagate much more slowly than the long waves, as expected. Note, however, that nonlinear effects that are not modeled here would damp these nonlinear short waves on a very short spatial scale (e.g., § 2.3.1). The rate at which the disk damps the simulated satellite's eccentricity e_s is shown in Figure 5, which compares well with the expected rate, equation (66).

The numerical quality of this simulation is assessed by monitoring the systems' total angular momentum deficit, which is $L_e = \frac{1}{2}\sum_j m_j n_j a_j^2 e_j^2$, where the sum runs over all rings and satellites in the system. Since this quantity is conserved by equations (2) (Hahn 2003), it provides a useful check on the simulation's numerical precision. The single-precision calculation shown in Figure 3 conserves L_e with a fractional error of $|\Delta L_e/L_e| < 4 \times 10^{-5}$.

4.2. Reflection at an Outer Boundary

Section 2.3.1 showed that ring viscosity is only marginally effective at damping the long waves that an eccentric satellite would launch at the gap's outer edge. Consequently, these waves will propagate outward until they hit a barrier, such as another gap in the ring or the ring's outer edge. The subsequent fate of
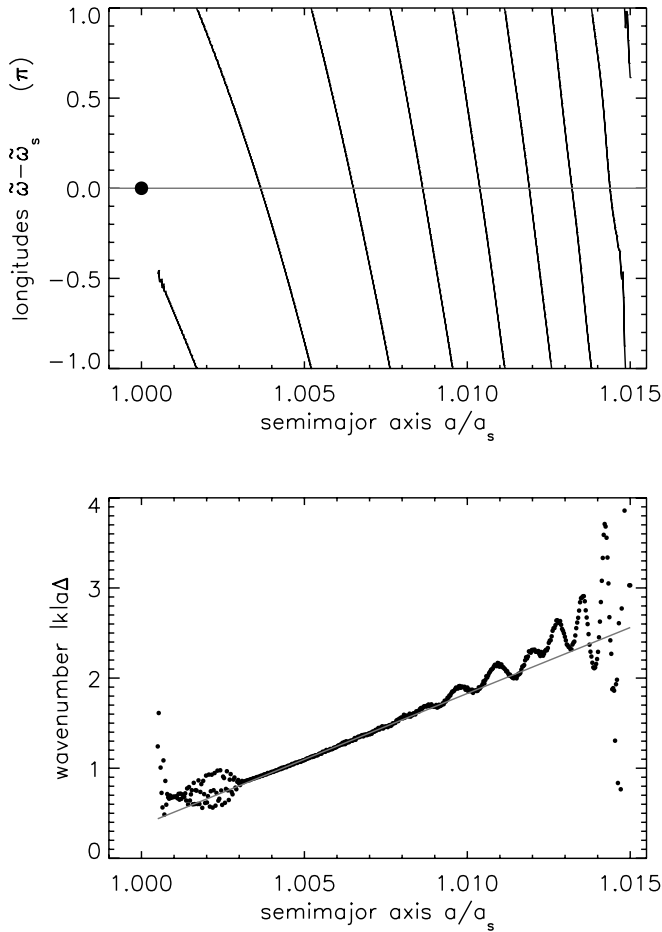
Fig. 4.—*Top*: Disk's longitude of periapse $\tilde{\omega}(a)$ relative to the satellite's periapse $\tilde{\omega}_s$, in units of π, for the simulation of Fig. 3 at time $t = 60 \times 10^3$ orbits, when the wave has swept across the disk. The dots in the bottom panel show the dimensionless wavenumber $|k|a\Delta$ at this moment, where wavenumber is calculated from $k = -\partial\tilde{\omega}/\partial a$. The gray line is the expected wavenumber, eq. (47), with $\varepsilon = 1$.

such a wave train is illustrated in Figure 6, which shows the state of the simulation described in § 4.1 but at a later time, $t = 2.1 \times 10^5$ orbits. Here, the outbound long wave has already reflected at the simulated ring's outer edge and propagated back toward the satellite, but as the superposition of a long leading wave and a short trailing wave. Consequently, the long-wavelength undulations seen in Figure 6's $e(a)$ curve represents the superposition of outbound and inbound long waves. Note, however, that the reflected waves' angular momentum content is now shared between a long and a short wave, so the amplitude of the inbound long wave is smaller than the outbound long wave. Consequently, the broad $e(a)$ undulations seen in Figure 6 are not due to a standing wave in the disk, but instead represent the superposition of two traveling waves having different amplitudes.

The high-frequency variations seen in Figure 6's $e(a)$ curve are due to short waves that have a wavelength that is comparable to the disk scale height h. Note that the right-hand side of Figure 6 shows that the reflected short wave is still confined to the vicinity of the ring's outer edge by time $t = 2.1 \times 10^5$ orbits, which indicates that these short waves travel slower than the long waves, as expected. The rapid variations in $e(a)$ seen at the left-hand side of Figure 6 show that the satellite is also exciting short waves at the gap's inner edge. These short waves are propagating much more slowly (see § 2.2.2), by a factor of $He^{-H} \sim 0.01$, so these very slow moving waves have had little oppor-
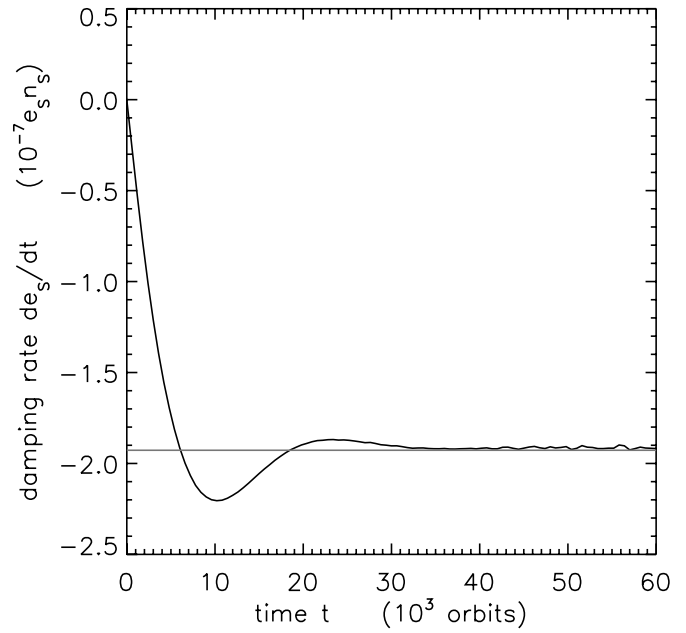

Fig. 5.—Rate at which the satellite launching the wave in Fig. 3 has its eccentricity damped, $\dot{e}_s$, plotted vs. time t in units of 10^3 orbit periods. The solid gray curve is the expected rate, eq. (66).

tunity to travel very far by time $t = 2.1 \times 10^5$ orbits. Longer term simulations also show that the amplitude of any short waves is always comparable to the amplitude of the long waves. Equation (54) also indicates that these short waves will be very nonlinear ($|\Delta\sigma/\sigma| > 1$), so the reflected short wave is expected to damp over a very short spatial scale that is probably comparable to the ring's scale height h, in the vicinity of the ring's outer edge.

However, the reflected long wave will still return to the disk's inner edge, where it can interact with the satellite and/or reflect again. The satellite can interact with this returning wave by absorbing some of the wave's angular momentum content, which would also excite the satellite's eccentricity and seemingly stall any further e-damping. However, that e-pumping would then be counterbalanced by enhanced eccentricity damping due to the excitation of even higher amplitude density waves. Consequently, the damping of the satellite's eccentricity by this phenomenon is still assured, despite the fact that long waves propagate with only a modest amount of viscous damping. This is due to the fact that all long waves eventually reflect somewhere in the disk and spawn short waves that are easily damped.

4.3. *Waves Launched by Pan*

The rings code is also used to simulate the density waves that an eccentric Pan can launch at the outer edge of the Encke gap. As § 2.3 notes, the ratio of the critical mass μ_c to the disk mass μ_d is $\mu_c/\mu_d \simeq 1.8$, which indicates that the wavenumber changes substantially over the first wavelength (see eq. [47]), which violates a key assumption in the derivation of the wave amplitude. In fact, a comparison of equation (52) to simulations of Pan's waves shows that that equation overestimates the wave amplitude by a factor of $\gamma \simeq 4$, which means that equation (66), which provides the satellite's eccentricity-damping rate, would also be in error by a factor of γ^2. Nonetheless, a comparison of the simulated wave's wavenumber $|k|$ to equation (47) shows that equation to be in excellent agreement with the model results. Equation (65) is also shown to be a reliable indicator of the satellite's eccentricity damping rate, even when $\mu_c > \mu_d$.
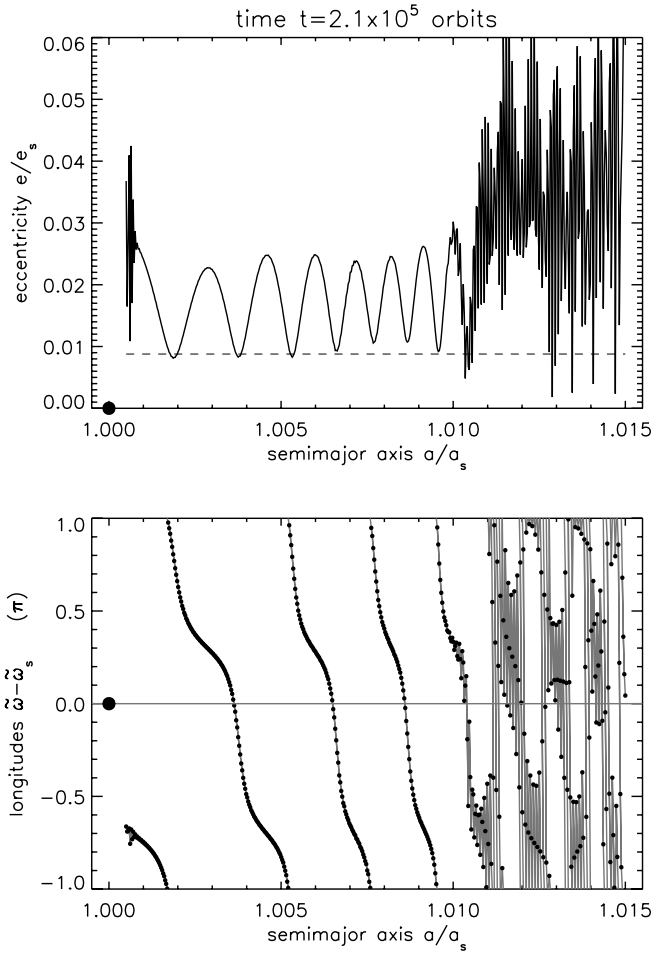
Fig. 6.—Simulation described in § 4.1 and Figs. 3–5 extended to time $t = 2.1 \times 10^5$ orbits. During this time, the outbound long wave has since reflected at the simulated disk's outer edge at $a/a_s = 1.015$ as a superposition of inbound long and short density waves. The long-wavelength undulations seen in $e(a)$ thus represent the superposition of the outbound and inbound long waves, while the high-frequency variations in $e(a)$ are due to the slower moving short waves. See § 4.2 for details.

These same simulations also show that density waves launched by Pan are not able to propagate across the Keeler gap, which lies about 2900 km downstream of the Encke gap. The width of that gap is approximately 40 km, which is about half the wavelength of Pan's waves in this region. Despite having a wavelength that is larger than the gap's full width, Pan's waves are unable to propagate across the Keeler gap. Instead, those waves reflect at the gap's inner edge, which, in the simulation, propagate back to Pan as a superposition of long and short waves. However, in a real disk those nonlinear short waves would quickly damp very near the Keeler gap's inner edge.

This wave action will also damp Pan's eccentricity over a timescale equal to equation (67) multiplied by $\gamma^2 = 16$, which evaluates to $\tau_e \simeq 1400$ yr. Note that this e-damping is competitive with, but not quite faster than, the eccentricity excitation that is due to Pan's Lindblad resonances in the ring, which pump up the satellite's e over a slightly faster timescale of $\tau_L \simeq 900$ yr (see eq. [71]). But if the particles' motions at Pan's corotation resonances are saturated, then e-damping by the corotation torque is shut off, while the e-excitation due to the Lindblad torque is halved (Goldreich & Tremaine 1981), so $\tau_L \rightarrow 1800$ yr. So when Pan's corotation resonances are saturated, Pan's e-damping due to its secular interaction with the ring will exceed the e-excitation

that is due to its Lindblad resonances in the ring, but only by a small margin. But if particle motions at Pan's corotation resonances are in fact unsaturated, then the near-cancellation of the Lindblad and corotation torques results in a secular e-damping timescale that is about 13 times shorter than the total resonant e-damping timescale (eq. [73]). In this case, e-damping by the secular interaction is the dominant process that stabilizes Pan's eccentricity.

Since this eccentricity damping due to wave excitation is so vigorous, one might wonder why Pan would even have a non-zero eccentricity. However, as Spitale et al. (2006) point out, the satellite Prometheus has a $16:15$ resonance that does disturb Pan, which may be responsible for sustaining Pan's eccentricity and the density waves that that satellite would launch at the outer edge of the Encke gap.

5. SUMMARY AND CONCLUSIONS

The Lagrange planetary equations are used to study the secular evolution of a small planetary satellite as it orbits within a narrow gap in a broad, self-gravitating planetary ring. These equations show that an eccentric satellite's secular perturbations of the nearby gap edge tend to excite very long wavelength spiral density waves that propagate out to greater distances in the ring. These results are applied to the two small Saturnian satellite's Pan and Daphnis, which inhabit narrow gaps in the main A ring. It is shown that these satellites can launch very low amplitude ($\Delta\sigma/\sigma < 0.4\%$) long waves whose wavelengths would be of order $\lambda \sim 100$s of km. The wavelength of these waves also shrinks with distance due to the central planet's oblateness, which causes the spiral pattern to wind up as the waves propagate. It is also shown that these long waves suffer only a modest amount of viscous damping as they propagate toward the A ring's outer edge. A dispersion relation is derived for these waves, which shows that a gap-embedded satellite can also excite short waves whose wavelength is comparable to the ring's scale height h. However, these short waves are very nonlinear ($\Delta\sigma/\sigma \sim 1$) and will damp soon after their excitation.

The Lagrange planetary equations are also used to derive the amplitude and wavelength of the long waves, as well as the rate at which this wave excitation tends to damp the satellite's eccentricity. However, these analytic results are only valid when the wavenumber k varies slowly across the first wavelength, which requires the so-called critical mass μ_c to be sufficiently small. Equation (46) shows that that occurs when the gap is sufficiently narrow or when the central planet's oblateness is sufficiently small. If, however, this requirement is not satisfied, then the rings model of Hahn (2003) can still be used to determine these waves' properties and the rate at which this wave action also damps the satellite's eccentricity. Note that the amplitude of these waves is proportional to the satellite's eccentricity, so this e-damping also tends to terminate subsequent wave generation.

The rings model shows that these undamped long waves will eventually reflect at the ring's outer edge (or at another gap in the ring), which then spawns both long and short waves that propagate inward. Since wave reflections eventually transmute all long waves into easily damped short waves, this process communicates the wave's angular momentum content to the ring itself, which also ensures that this wave phenomenon ultimately damps the satellite's eccentricity, too.

This eccentricity damping due to wave excitation is then compared to the e-evolution rates that are due to the satellite's interaction with ring material orbiting at its Lindblad resonances

(which tends to pump up the satellite's eccentricity) and corotation resonances (which tends to damp the satellite's eccentricity). It is shown that e-damping due to wave excitation is the dominant process when the gap width is sufficiently wide (see eq. [74]). For the case of Pan, these e-damping and e-excitation rates are all comparable to each other, but Daphnis's e-evolution is dominated by the Lindblad and corotation torques. And since Daphnis's long-term orbital stability requires e-damping to dominate over e-excitation, these results also imply that particle motions at Daphnis's corotation resonances are unsaturated, which is necessary for the corotation torque to be operative here.

REFERENCES

Abramowitz, M., & Stegun, I. A. 1972, Handbook of Mathematical Functions (New York: Dover)
Binney, J., & Tremaine, S. 1987, Galactic Dynamics (Princeton: Princeton Univ. Press)
Borderies, N., Goldreich, P., & Tremaine, S. 1985, Icarus, 63, 406
Brouwer, D., & Clemence, G. M. 1961, Methods of Celestial Mechanics (New York: Academic)
Daisaka, H., Tanaka, H., & Ida, S. 2001, Icarus, 154, 296
Goldreich, P., & Sari, R. 2003, ApJ, 585, 1024
Goldreich, P., & Tremaine, S. 1981, ApJ, 243, 1062
———. 1982, ARA&A, 20, 249
Hahn, J. M. 2003, ApJ, 595, 531
———. 2007, ApJ, 665, 856
Jacobson, R. A., Spitale, J., Porco, C. C., Beurle, K., Cooper, N. J., Evans, M. W., & Murray, C. D. 2008, AJ, 135, 261

Murray, C. D., & Dermott, S. F. 1999, Solar System Dynamics (Cambridge: Cambridge Univ. Press)
Porco, C. C., Thomas, P. C., Weiss, J. W., & Richardson, D. C. 2007, Science, 318, 1602
Porco, C. C., et al. 2005, Science, 307, 1226
Shu, F. H. 1984, in IAU Colloq. 75, Planetary Rings, ed. R. Greenberg & A. Brahic (Tucson: Univ. Arizona Press), 513
Spitale, J. N., Jacobson, R. A., Porco, C. C., & Owen, Jr., W. M. 2006, AJ, 132, 692
Tiscareno, M. S., Burns, J. A., Nicholson, P. D., Hedman, M. M., & Porco, C. C. 2007, Icarus, 189, 14
Tiscareno, M. S., Hedman, M. M., Burns, J. A., Porco, C. C., Weiss, J. W., & Murray, C. D. 2005, AGU Abstr. Fall, B245
Toomre, A. 1964, ApJ, 139, 1217
———. 1969, ApJ, 158, 899